



Geology, Vein Textures, and Fluid Inclusions of the Cibeber Low-Intermediate Sulfidation Epithermal Au-Ag Orefield, Western Java

CENDI D. P. DANA¹, ARIFUDIN IDRUS^{1*}, IWAN SETIAWAN², ESTI HANDAYANI³, FEDDY YURNIADI⁴,
IGNAS A. MEAK⁴, and CHUN-KIT LAI⁵

¹Department of Geological Engineering, Universitas Gadjah Mada, Yogyakarta, Indonesia

²Geotechnology Research Center, Indonesian Institute of Sciences, Bandung, Indonesia

³Research and Development Centre for Mineral and Coal Technology,
Ministry of Energy and Mineral Resources, Bandung, Indonesia

⁴PT. Multi Utama Kreasindo Mining, Lebak, Indonesia

⁵Faculty of Science, Universiti Brunei Darussalam, Brunei Darussalam

Corresponding author: arifidrus@ugm.ac.id

Manuscript received: August 19, 2020; revised: September 12, 2020;

approved: October 23, 2020; available online: May 18, 2021

Abstract - This paper describes the results of surficial geological and alteration mapping combined with several laboratory analyses, including petrography, ore microscopy, ore geochemistry, and fluid inclusion studies, aimed at establishing the nature of mineralization and alteration in the Cibeber area, West Java, Indonesia, and developing a genetic model. The area forms part of the Bayah Dome Complex, which hosts several gold-silver deposits. It is underlain by andesitic lava, tuff breccia, and subordinate sandstone. Its structural framework consists of joints, normal faults, NE-SW dextral strike-slip faults, and NW-SE strike-slip faults. Hydrothermal alteration can be divided into four types, viz. silicification, clay-silica, argillic, and propylitic. Mineralization is mostly hosted in quartz veins showing a variety of textures, including massive, colloform-crustiform, breccia, lattice bladed, comb, and saccharoidal. Ore minerals consist of native gold and silver, pyrite, chalcopyrite, sphalerite, galena, tennantite-tetrahedrite, covellite, malachite, hematite, and goethite, while the gangue minerals quartz, illite, epidote, and calcite. Four stages of mineralization/veining are recognized: early, middle (the main ore forming stage), late, and supergene. The highest obtained metal grades are 8.17 ppm Au, 113.6 ppm Ag, 1.23% Cu, 1.28% Pb, and 1.2% Zn. Fluid inclusions from mineralized veins yielded temperatures of 222 - 280°C and salinities of 0.36 - 1.31 wt.% NaCl eq. The hydrothermal fluids are interpreted to have been largely of meteoric origin with the mineralization having formed at a depth of about 258 - 270 m below paleosurface. Both low-sulphidation and intermediate-sulphidation styles of mineralization are present.

Keywords: fluid inclusion, epithermal, gold-silver, vein texture, Cibeber

© IJOG - 2021.

How to cite this article:

Dana, C.D.P., Idrus, A., Setiawan, I., Handayani, E., Yurniadi, F., Meak, I.A., and Lay, C.K., 2021. Geology, Vein Textures, and Fluid Inclusions of the Cibeber Low-Intermediate Sulfidation Epithermal Au-Ag Orefield, Western Java. *Indonesian Journal on Geoscience*, 8 (2), p.157-175. DOI: [10.17014/ijog.8.2.157-175](https://doi.org/10.17014/ijog.8.2.157-175)

INTRODUCTION

The Java metallogenic belt in Indonesia is one of the most prospective gold-silver belts in SE Asia (Prihatmoko and Idrus, 2020). The Bayah Dome Complex in western Java, in particular, hosts a number of important epithermal Au-Ag

deposits, such as Gunung Pongkor, Cibaliung, and Cikotok (Figure 1) (Leeuwen, 1994; Sunarya, 1997; Angeles *et al.*, 2002; Warmada, 2003; Harijoko *et al.*, 2007; Rosana, 2009). Cibeber, located about 9.5 km from the Cikotok deposit (Lebak Regency, Banten Province, Indonesia), is a newly discovered ore field in the belt. The

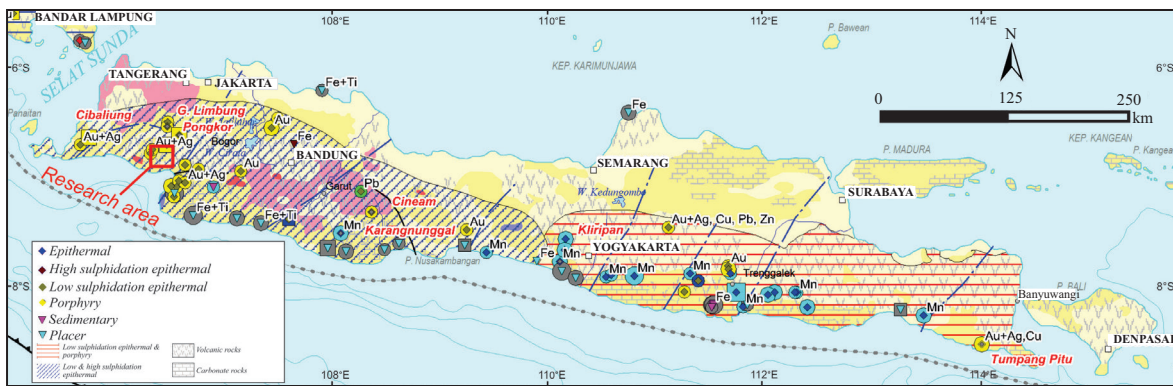


Figure 1. Location map of the Java metallogenic belt, showing the distribution of major ore fields associated with pre-Quaternary volcanism. Note that the western Java is mostly dominated by epithermal-type deposits, whilst the eastern Java is dominated by porphyry-type deposits (modified after Harahap *et al.* 2013).

exploration has been started since 1990's by PT Aneka Tambang and Atapa Minerals Ltd., focusing on the southern part of this area. Currently, the underground mining activities and smelting process are carried out by the management of PT Multi Utama Kresindo Mining since 2008. New wide gold bearing veins were also discovered recently in 2011 in northern part of the area. Previous studies mainly described the different mineralization styles in the dome complex and grouped them into five types, namely the Pongkor, Cirotan, Cikotok-Cikidang, Cisungsang, and Cibaliung type (Marcoux and Milesi, 1994; Widi, 2007; Rosana, 2009). However, there is no mineralogical or fluid inclusion data were reported from this studied area. In this study, an integrated study on the structural geology, hydrothermal alteration, ore mineralogy, and fluid inclusions associated with the mineralization at Cibeber is presented, and its genetic model and exploration implications are discussed.

MATERIALS AND RESEARCH METHODS

Detailed geological and alteration mapping were conducted at and around the Cibeber deposits (across a 12 km² area) aimed at observing relevant geological features and delineating lithological and alteration boundaries. Altered rock and epithermal vein samples were collected from outcrops and mining tunnels. Fifteen wall-rock and three vein samples were prepared for

petrographic thin sections, and twenty-three vein samples for polished thick sections. Ore macro-/micro-petrographic observations were carried out in the Laboratory of Optical Geology at the Department of Geological Engineering, Gadjah Mada University, with a Euromex trinocular polarizing microscope. Petrographic identification was based on standard mineral properties of rock forming minerals described by Barker (2014) and ore mineral optical properties by Marshall *et al.* (2004). Six altered rocks were X-Ray Diffractometry (XRD) analyzed at the Central Laboratory of the Department of Geological Engineering (Gadjah Mada University), using a Rigaku Multiflex 2KW Diffractometer. Three different treatments were performed namely bulk rock, air-dried, and ethylene glycollated. Peak identification was carried out manually based on the table of key line standards of Chen (1977). Thirty-three ore vein and twenty-two host-rock samples were analyzed by Fire Assay-Atomic Absorption Spectroscopy (AAS) at the laboratory of PT Multi Utama Kresindo Mining. Gold-silver contents were analyzed with the wet method using aqua regia digestion (HCl:HNO₃ = 3:1). Base metals were analyzed and dissolved in a mixture of perchlorate acid, nitric acid, and hydrochloric acid. The detection limits of Au, Ag, Cu, Pb, and Zn are 0.02, 0.50, 2.00, 4.00, and 2.00 ppm, respectively. Representative polished thin sections were analyzed with Scanning Electron Microscope – Energy Dispersive X-Ray Spectroscopy (SEM-EDS) for the mineral contents, using a JEOL JSM.6360

LA SEM with a JED-2200 Series EDS instrument operated at a 20kV accelerating voltage. The SEM-EDS analysis was carried out at the Research and Development Centre for Mineral and Coal Technology. Ore minerals such as pyrite, chalcopyrite, galena, and sphalerite were analyzed through point analyses for elemental identification. Semi-quantitative analyses were performed using ZAF correction with detection limits of 0.01 wt.%. Reference samples of similar composition (pyrite, chalcopyrite, galena, and sphalerite) were used for monitoring the accuracy of analyses. Five quartz vein samples with different textures and mineral assemblages were analyzed for their fluid inclusions, using a non-destructive method and double polished wafer preparation technique. The analysis was carried out at the Laboratory of Physical Mineral, Geotechnology Research Centre, Indonesian Institute of Science, with a Nikon Optihot 2 polarized microscope equipped with a Linkam THMS 600 heating-freezing stage. Ho-

mogenization and ice melting temperatures were determined with accuracy of +/- 2°C. Temperatures of homogenization above 200°C were measured with precision of +/- 1°C and temperatures below 200°C (homogenization and melting) with precision of +/- 0.1°C. Salinity was calculated based on the formula proposed by Potter (1977).

RESULTS AND DATA

Geological Setting

The Cibeber deposits/ore field, and other deposits in the Bayah Dome Complex are part of a calc-alkaline magmatic arc, which started to develop probably in the Paleogene in an active continental margin setting (Bemmelen, 1949; Whitford, 1975). The Bayah Dome Complex is a volcanic centre, which comprises the Cikotok Formation, Jampang Volcanics, and the Cihara Granodiorite (Figure 2). The Cibeber epithermal deposits are

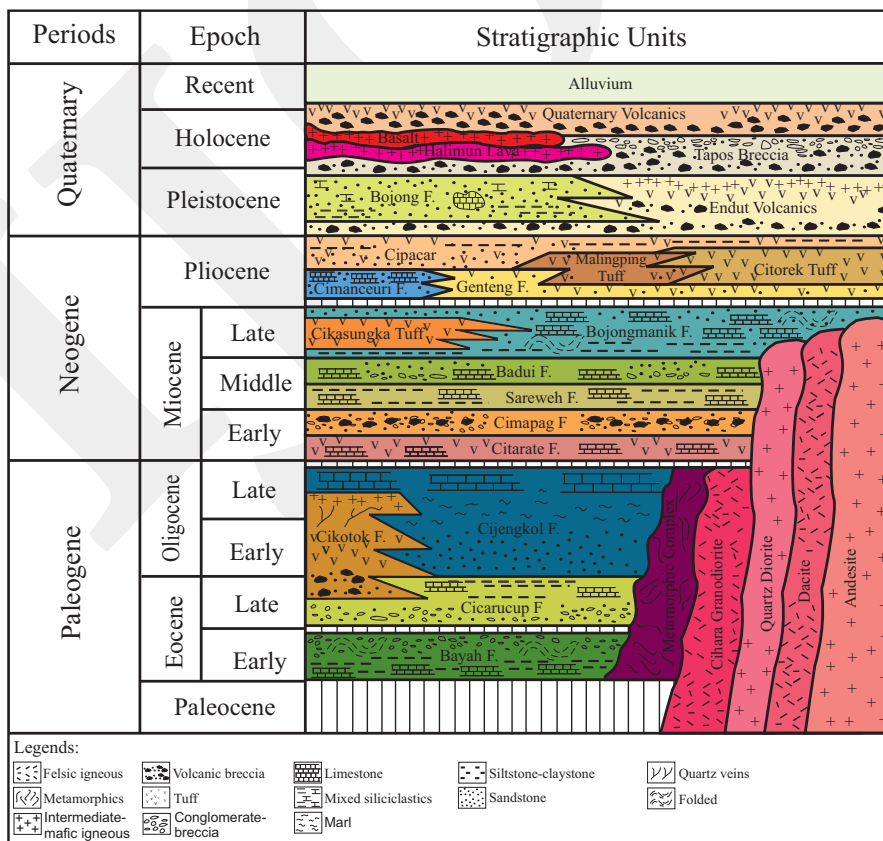


Figure 2. Regional stratigraphic column of the Bayah Dome Complex and its various intrusive phases where Cikotok Formation is the main ore host in the area (modified after Sujatmiko and Santosa, 1992).

hosted in volcanic breccia/tuff and andesitic lava of the Upper Eocene-Upper Oligocene Cikotok Fm. (Sujatmiko and Santosa, 1992). At Cibeber, these rock types are mostly altered and intruded by mineralized and barren quartz veins. Geochemical analyses show that the Cikotok Formation formed in an island-arc setting (Hutabarat, 2016). The Upper Eocene Cicarucup Formation is composed of conglomerate, quartz arenite, claystone, tuff, and limestone. Pulungguno and Martodjojo (1994) reported three structural patterns on Java Island, *i.e.*, Late Cretaceous NE-trending structures (termed the Meratus Pattern), Early Eocene-Late Oligocene N-S-trending structures (termed the Sunda Pattern), and Mio-Pliocene E-W-trending structures (termed the Java Pattern). At Cibeber, only the Java Pattern (represented by E-W trend-

ing thrust faults and folds) and the Sunda Pattern (represented by N-S trending strike-slip faults) were observed.

Geology of The Cibeber Deposits

The following geological description of the Cibeber deposits is mainly from Dana *et al.* (2018a and 2018b) with some additional data. The Cibeber deposits are hosted in three rock units from three different major rock formations, which are from old to young: (1) Cicarucup Fm. sandstone-mudstone, (2) Cikotok Fm. tuffaceous breccia, and (3) Cikotok Fm. andesitic lava (Figure 3). Andesitic lava is also locally found intercalated in the tuffaceous breccia. Formations (2) and (3) have typical subaerial volcanic features and can be classified as proximal volcanic facies. The ore veins are

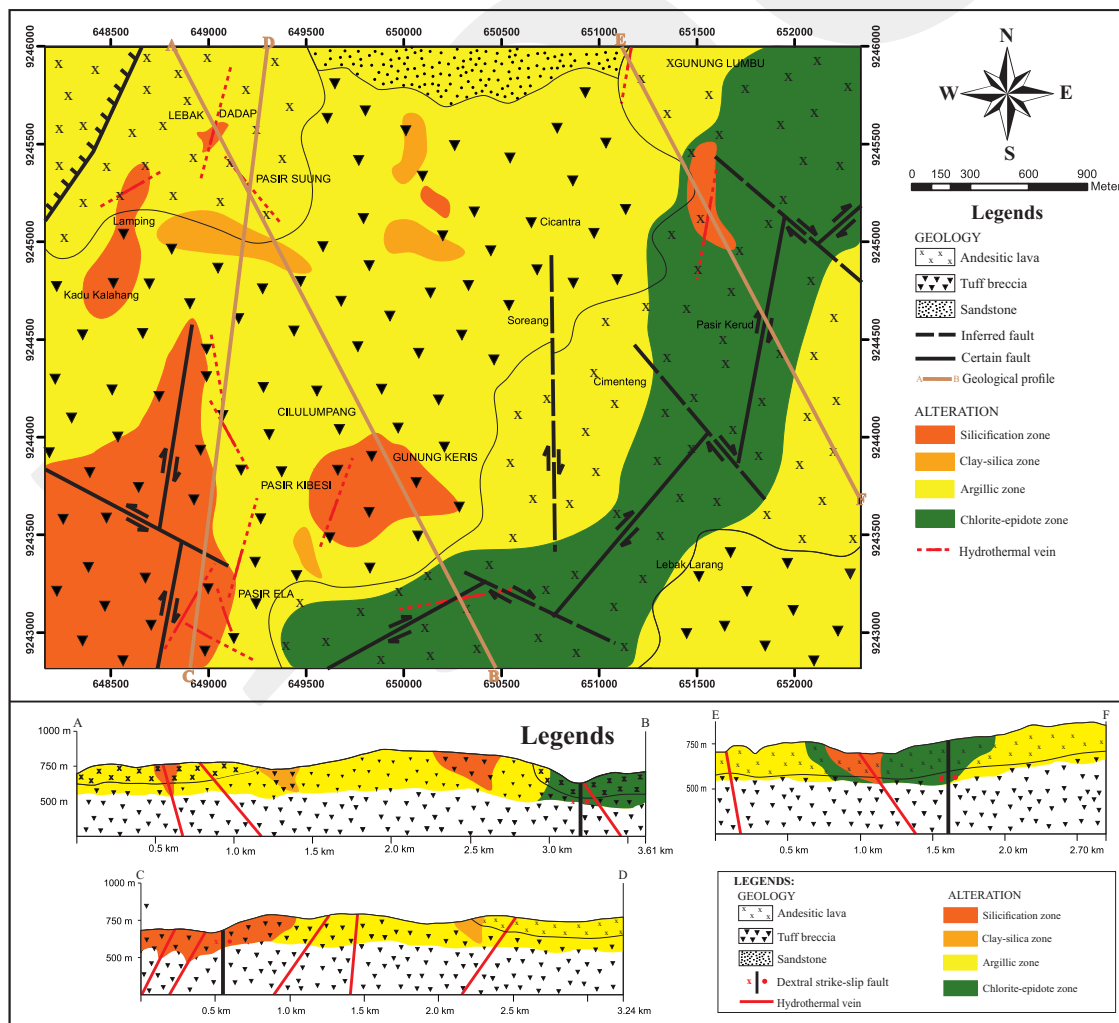


Figure 3. Geological and alteration maps of the Cibeber gold deposits (Dana *et al.*, 2018a and 2018b).

hosted by the intensely-altered tuffaceous breccia and andesitic lava, in which most of the primary minerals were replaced by secondary quartz, illite, chlorite, and epidote. Remnants or pseudomorphs of clinopyroxene and plagioclase phenocrysts are locally recognizable in the andesitic lava. Major structures at Cibeber are dominated by NNE-SSW strike-slip faults as well as some extensional and shear joints. The extensional and shear joints are NE-trending. The faults can be divided into pre-ore, syn-ore, and post-ore. The pre-ore NE-trending normal faults are possibly related to caldera formation in the Bayah Dome Complex. The syn-ore NNE-trending dextral strike-slip faults have formed other dilational structures in the area, which is quite common structural features found in epithermal system (*e.g.* Corbett and Leach, 1996; Garwin *et al.*, 2013; Corbett, 2013), whilst the post-ore NW-trending dextral strike-slip faults cut the syn-ore structures. Cooling/decompression structures such as sheeting and columnar joints were also observed in the andesitic lava unit.

Alteration Types and Distribution

The following description of hydrothermal alteration of Cibeber deposits is mainly from Dana *et al.* (2018a and 2018b) with some additional data. Three hydrothermal alteration styles have been identified, namely (1) propylitic (chlorite+epidote+illite+calcite \pm palygorskite), (2) argillic (illite+quartz \pm chlorite), and (3) silicic (quartz+crystalalite \pm halloysite). Mineral assemblages of these three alteration styles were determined by optical petrographic observations and XRD analyses.

Propylitic alteration occurs dominantly in the periphery of the deposits, mainly associated with the andesitic lava unit (Figure 3). Pyrite is common occurring as disseminations or in fine stockworks, whilst magnetite is patchy. Epidote and chlorite mostly replace clinopyroxene and plagioclase, but epidote can also be found as veinlets in some outcrops. The original igneous intergranular and trachytic texture is still partially preserved (Figure 4). Argillic alteration is well-developed in

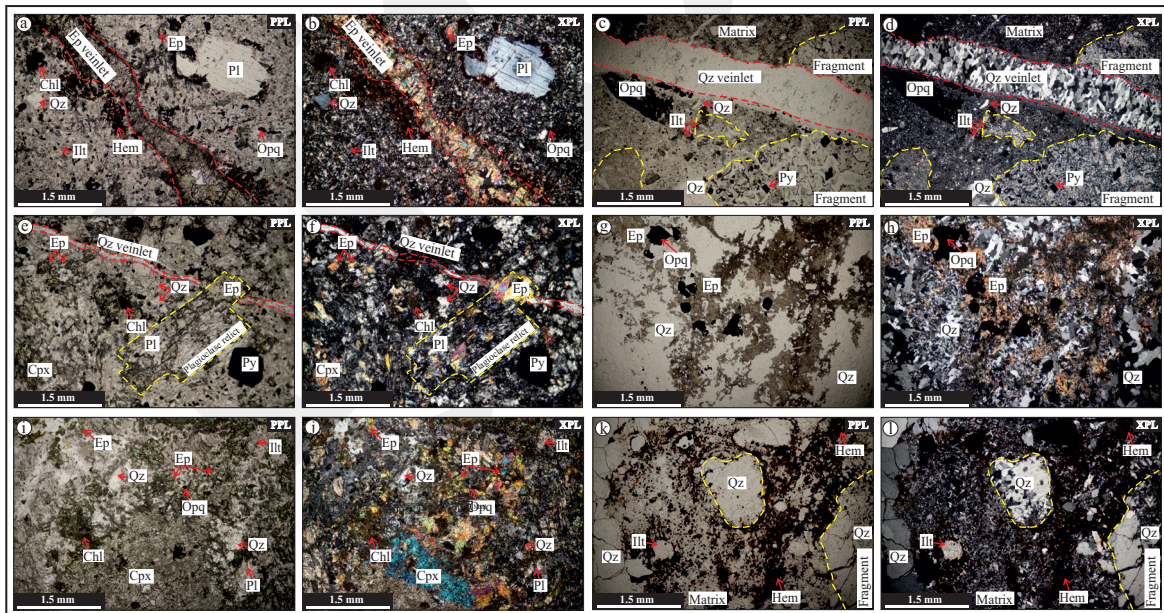


Figure 4. Photomicrographs of the different alteration styles at Cibeber. (a-b) Epidote veinlet in selectively-altered andesitic lava with primary quartz and plagioclase; (c-d). Quartz-clay replacement in tuffaceous breccia with comb-textured quartz veinlet; (e-f). Clasts are mostly replaced by clay and groundmass by microcrystalline quartz. Disseminated pyrite are common; Epidote-chlorite alteration, with quartz veinlet in andesitic lava and relict texture; (g-h). Sericite replaced both feldspar phenocrysts and groundmass; Quartz-epidote vein with disseminated sulfide (dominantly galena and sphalerite) mineralization; (i-j). Epidote almost entirely replaced clinopyroxene phenocrysts in the andesitic lava; (k-l). Some plagioclase laths also remain in the selectively chlorite-sericite-altered groundmass; Intense oxidation indicated by hematite-rich tuffaceous breccia, whose clasts are mostly replaced by quartz. Abbreviations: Ep: epidote; Ill: illite; Qz: quartz; Hem: hematite; Pl: plagioclase; Chl: chlorite; Py: pyrite; Opq: opaque minerals; Cpx: clinopyroxene.

tuffaceous breccia, and locally in a highly-fractured andesitic lava. This alteration style is characterized by pervasive clay and quartz replacement, except in the Cicarucup sandstone and claystone, due to their higher quartz content and lower permeability. XRD analysis indicates that some primary minerals (*e.g.* plagioclase and K-feldspar) still remain in the altered rocks (Dana *et al.*, 2018a; Figure 5).

Silicic alteration is characterized by pervasive silica replacement, which comprises mostly quartz and minor cristobalite and chalcedony, as indicated by XRD analysis. This alteration zone occurs mostly as halos along the quartz veins, except at Cirahong and Curug Engang where the alteration is pervasive. Many silicic-altered rocks were also later oxidized, as indicated by the reddish hematite stain.

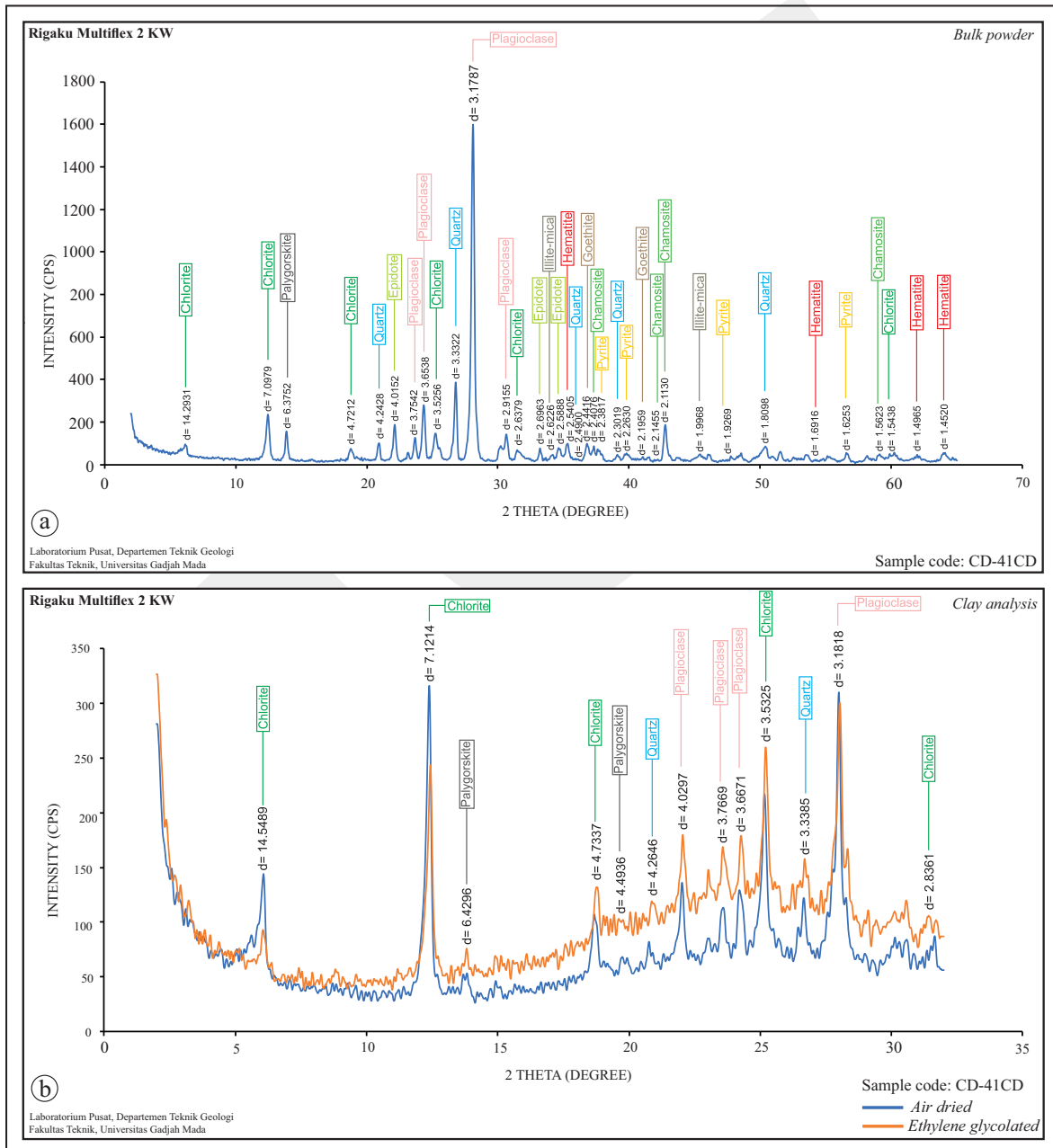


Figure 5. (a). XRD results of the propylitic-altered Cikatok Fm. andesitic lava at Cibeber (Dana *et al.*, 2018a). Alteration minerals include mainly chlorite, epidote and illite, and minor palygorskite (altered from plagioclase). The different chlorite-group mineral is identified as chamosite. The three opaque minerals identified are hydrothermal pyrite, and supergene hematite and goethite. (b). SEM-EDS results of some representative mineral samples from Cibeber.

Hydrothermal Vein System and Ore and Gangue Mineralogy

Hydrothermal veins were found across the studied area. Mineralized veins are commonly thicker than ore-barren veins, occurring in the form of massive veins, stockworks, and hydrothermal breccias (Dana *et al.*, 2018a; Figure 6). The following is a description of the features of hydrothermal veining in the three major prospects at Cibeber (*i.e.* Lebak Dadap, Cilulumpang, and Pasir Ela).

Lebak Dadap Prospect

This area is characterized by hydrothermal breccia stockwork, comprising three main vein systems (*i.e.* Lebak Dadap, Lamping, and Pasir Suung). The veins are mostly mineralized composed of pyrite-oxide-rich with minor base metal sulfides; some ore-bearing and barren veins have comb textures. The Lebak Dadap veins are N-S-trending and ~1.5 m thick, the Lamping veins are NE-trending and ~1 m thick, whilst the Pasir Suung veins are NW-trending and also ~1 m thick. The Pasir Suung veins have lattice bladed textures, with quartz, calcite, and chlorite as the dominant gangue minerals.

Cilulumpang Prospect

The area comprises the Cilulumpang Vein Complex and the Gunung Keris vein system. These veins are generally 1 m thick and variably textured. The Cilulumpang Vein Complex has a massive and saccharoidal texture and a NNW-strike. Lattice bladed texture can also be seen. Microcrystalline quartz and illite-sericite are the most common gangue minerals. The Gunung Keris veins are characterized by their lattice bladed texture, relatively low ore mineral contents, and with quartz and chalcedony as the dominant gangue minerals. The veins are commonly 1.5 m wide and NE-trending.

Pasir Ela Prospect

The area has three main vein systems, *i.e.* Cidikit, Curug Engang, and Pasir Ela. The Cidikit veins contain mainly massive quartz and base metal sulfides (mostly galena and sphalerite), and epidote. The veins are commonly 1 m wide and ENE-trending. The Curug Engang veins are thinner (0.25 m wide), NE-trending, and have a colloform texture. These veins have pyrite and base metal sulfides with quartz-calcite gangue. The Pasir Ela vein system includes both miner-

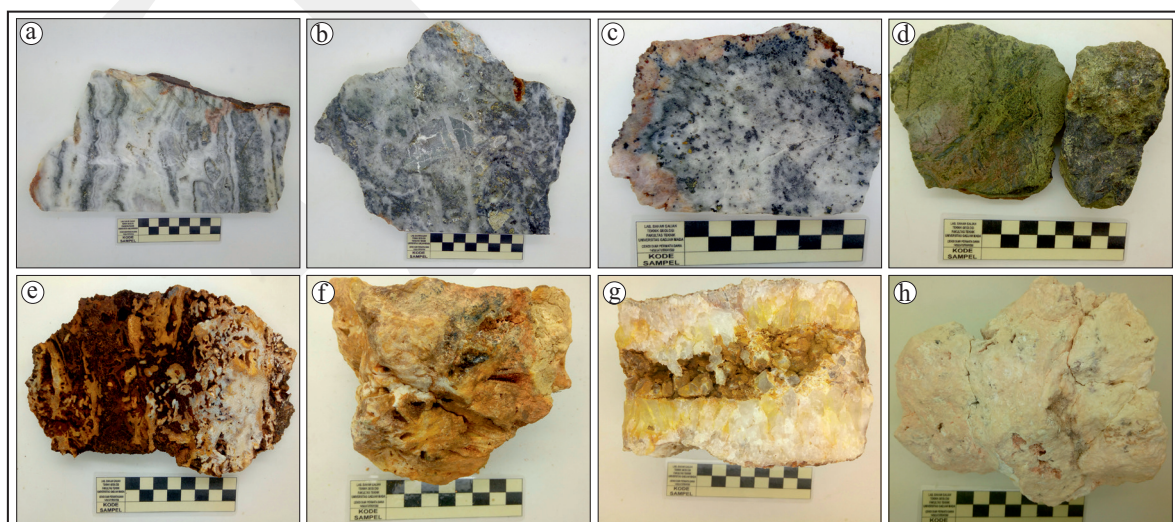


Figure 6. Hand-specimen photos of the hydrothermal quartz veins and photomicrographs of ore minerals in quartz veins from Cibeber (Dana *et al.*, 2018a), showing different textures including (a). colloform, (b). breccia, (c-d). massive, (e-f). lattice bladed, (e-f). comb, and (h). saccharoidal. Colloform and breccia veins are typically precious metal-rich, while massive veins are base metal-rich. Special epidote-base metal veins are also found, (d). Lattice bladed veins are commonly oxide-rich and low in both precious and base metal contents, whilst comb- and saccharoidal-textured veins are mostly barren.

alized and barren veins. The formers are mostly colloform-crustiform, containing mainly galena, sphalerite, and chalcopyrite. Supergene enrichment also occurs, as indicated by the presence of by covellite and malachite. The veins are 0.6 to 1.2 m thick and are NE- or NW-trending. Breccia veins are also locally found. Ore-bearing and barren veins (0.2 to 0.7m thick) comprise mostly quartz-chalcedony ± amethyst, and are dominantly comb (minor crustiform)-textured. The barren veins have various directions and represent a late-stage post-ore phase.

Ore Mineralogy and Geochemistry

Ore minerals in the studied area include hypogene and supergene ones. Representative sulfides (pyrite, sphalerite, chalcopyrite, and galena) were analyzed for their chemical compositions. Alteration/mineralization paragenesis was mostly determined based on the mineral assemblages and vein crosscutting relationships. Mineralization mostly

occurs in hydrothermal veins and to a minor extent in altered wall-rocks. Three major groups of ore minerals include Au-Ag-bearing sulfides, base metal sulfides, and supergene metallic minerals. Ore microscopic images of the various minerals are shown in Figure 7.

Base Metal Sulfides

Pyrite is the most abundant sulfide mineral at Cibeber. It is euhedral cubic (1–5 mm), and has an average content of 43.95 wt.% sulfur (S) and 55.17 wt.% Fe, together with 0.17 wt.% Cd, 0.13 wt.% Ag, and minor Co, Ni and Cu (0.1 wt.% each). Manganese was detected in only one sample (0.28 wt.%). Chalcopyrite is mostly found in the Pasir Ela, Curug Engang, Cidikit, and Citajin vein systems, and is associated with other base metal sulfides. It can be distinguished from pyrite by its lower reflectance. The chalcopyrite on average 26.86 wt.% S, 34.62 wt.% Fe, and 38.52 wt.% Cu. Galena (size: 1 - 5 mm)

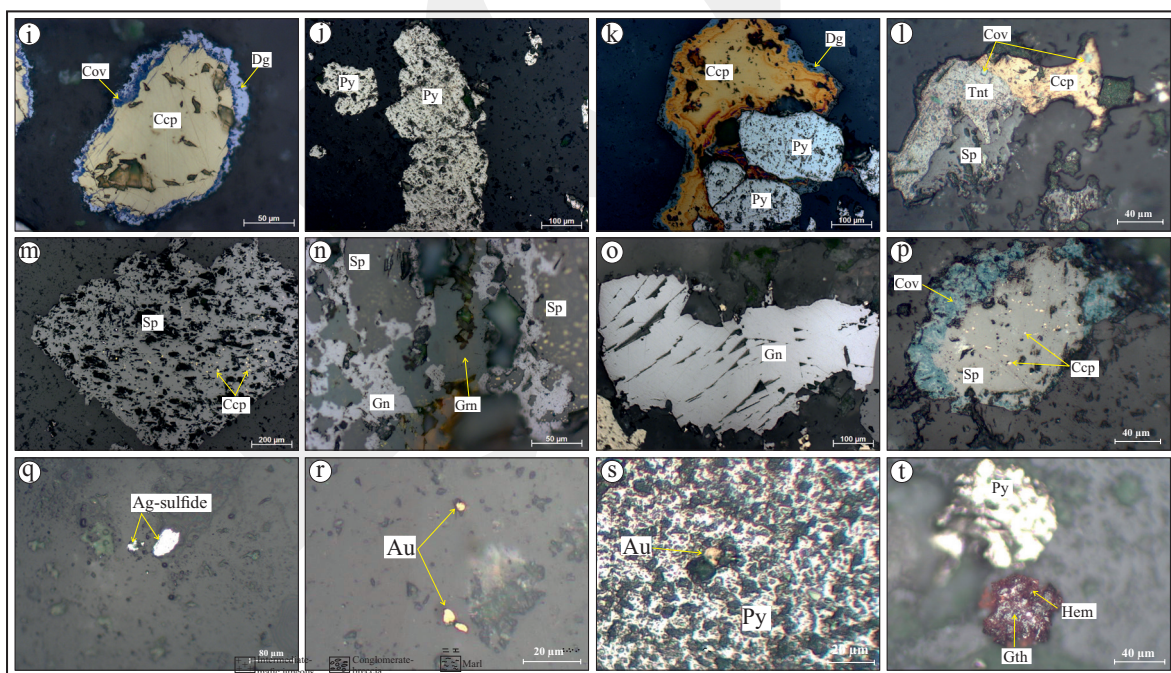


Figure 7. Ore microscopic images: (a, c). Covellite and digenite are found replacing the Cu-bearing minerals such as chalcopyrite; (b). Pyrite is the most common sulfide found either disseminated or aggregates; (d, f). Another minor ore mineral such as tennantite-tetrahedrite and greenockite also can be found; (e). Sphalerite is typically characterized by the presence of chalcopyrite disease (cf. Craig and Vaughan 1994); (g). Galena can be easily distinguished by the presence of triangular pits (cf. Marshall *et al.* 2004); (h). Covellite also can be found replacing the sphalerite as the consequence of chalcopyrite disease occurrences; (i, j). Gold and Ag-sulfide can be identified as free grain; (k). Gold also can be found as inclusion within pyrite; and (l). pyrite is oxidized to be hematite and goethite. Abbreviations: Py: pyrite; Cv: covellite; Dg: digenite; Ccp: chalcopyrite; Gn: galena; Sp: sphalerite; Grn: greenockite; Tnt: tennantite; Gth: goethite; Hem: hematite; Au: gold.

is mostly disseminated in quartz veins, which is easily distinguished under the microscope by its triangular pits. The galena from Cibeber has on average ($n=4$) 72.41 wt.% Pb and 27.35 wt.% S, and one sample has up to 0.99 wt.% Fe. Sphalerite (size: 1–200 μm) is found both as disseminations and in veins. “Chalcopyrite disease” texture (chalcopyrite exsolution lamellae in sphalerite) is commonly observed under the microscope. Sphalerite from Cibeber has a low Fe content (average 3.72 wt.%), and contains 70.31 wt.% Zn and 25.93 wt.% S. Other base metal minerals such as tennantite-tetrahedrite and greenockite are also present. They are very fine-grained (size: 10–80 μm) and associated with other base metal sulfides at Pasir Ela.

Gold-/Silver-bearing Sulfides

Precious metal minerals from Cibeber are in general very fine-grained (identifiable only under the microscope), although some visible free gold grains (size: 0.5–1 mm) were observed at Lebak Dadap. Gold can be found both as free grains and inclusions in pyrite. Silver sulfides, possibly acanthite (size: 10–40 μm), occur as disseminations in quartz veins, have only been identified in the Pasir Ela vein. No chemical analysis has been conducted of these minerals.

Supergene Minerals

The most common supergene minerals are hematite and goethite, probably formed from hypogene pyrite and magnetite. Intense oxidation is found mostly at Pasir Suung, where hypogene pyrite is abundant. Malachite and covellite are the most common Cu-bearing supergene minerals at Cibeber. Malachite is generally found in the supergene zone, along with other carbonate and sulfate minerals such as chrysocolla and chalcantite. Chalcocite and covellite are the major secondary Cu sulfides in the supergene zone. Malachite can be readily identified both in outcrop and in float samples, especially in the Pasir Ela prospect. Meanwhile, covellite is identified by its characteristic blue colour and brownish-red anisotropy. Optical microscopic analysis indicates

that covellite replaces chalcopyrite and sphalerite, and locally replaces pyrite.

Bulk-ore Metal Grades

Ore assay data were obtained from thirty-three vein and twenty-two altered wall-rock samples. Gold grades of the vein samples range from <0.02 to 8.17 ppm (average 0.8 ppm), with the highest grade found in the Curung Engang vein. The highest gold grade (0.45 ppm) in wall-rocks is found in the propylitic-altered andesitic lava. Silver grades range from 0.6 to 113.6 ppm (average 26 ppm) in the vein samples, and from 0.5 to 5.1 ppm in the wall-rock samples. The highest Ag grades occur in a colloform vein from the Pasir Ela prospect, and in a silicified andesitic lava sample in the Curug Engang. However, some samples, both vein and wall rock, have silver grades below the detection limit. Copper grades in the vein samples range from 9 ppm to 1.23%, and in the wall rock samples from 8 to 110 ppm. Lead grades in the vein and wall rock samples range from 34 to 1,280 ppm, and from 21 to 1,460 ppm, respectively. The vein samples contain 8 to 1,200 ppm Zn, while that of the wall rock samples 13 to 1,570 ppm. Base metal grade analyses were only carried out on samples with > 0.15 ppm gold grade. The highest base metal grades were found in colloform veins in the Pasir Ela prospect and in propylitic-altered andesitic lava around the Cidikit vein.

Fluid Inclusion Study

Fluid inclusions (FIs) from five quartz vein samples with different textures (massive, colloform, breccia, lattice bladed, and comb) were analyzed to characterize the ore-forming fluids. Most of the vein samples are mineralized, except for the lattice bladed- and comb-textured ones. Massive and colloform veins have much higher base metal sulfide contents than the breccia veins. Primary, secondary and pseudo-secondary FIs are all three found in all samples. Types of primary FIs include L-type (single-phase), LV-type (two-phase), and VL-type (two-phase) (Goldstein, 2003; Pirajno, 2010; Pohl, 2011).

Petrography and Fluid Inclusion Types

The comb vein sample (CV-01CJ) was taken from the Citajin area. Primary FIs (size: 3–15 μm) have various forms, including ellipsoid, rectangular, bipyramidal, and irregular. Necking is commonly observed in this vein. All three primary FI types are present. Secondary FIs are dominated by ellipsoidal LV-type, while pseudo-secondary FIs are dominantly bipyramidal and small.

The lattice bladed vein sample (CV-19GK) was taken from Gunung Keris area, characterized by very low metal content (0.1 ppm Au, <0.5 ppm Ag, 20 ppm Cu, 243 ppm Pb, 580 ppm Zn). Both primary and secondary FIs were observed in this sample. Most FIs are very small (2–10 μm) and irregularly-shaped. The FIs are dominantly LV-type. Meanwhile, L-type FIs were also observed in minor amounts and smaller than LV-type.

The breccia vein sample (CV-12LD) was taken from the Lebak Dadap area. This vein is pyrite rich and has relatively high metal contents (0.85 ppm Au, 5.6 ppm Ag, 450 ppm Cu, 84 ppm Pb, 335 ppm Zn). Pseudo-secondary FIs are difficult to distinguish from secondary FIs due to indistinct crystal growth lines in the quartz crystals. Primary FIs are smaller than secondary ones, and are dominated by ellipsoidal and irregular shapes. Both L-type and LV-type FIs were observed either as primary or secondary FIs.

The colloform vein sample (CV-02PE) was taken from the Pasir Ela area, that is characterized by high Ag and base metal contents (0.64 ppm Au, 113.6 ppm Ag, 12,300 ppm Cu, 410 ppm Pb, 10,200 ppm Zn). Petrographic analysis on five quartz bands reveals various forms of FIs (size: 3–30 μm), including ellipsoid, irregular, rectangular, and (bi)pyramidal. LV-type FIs are the most common FI type in the sample, and minor L-type FIs are also found.

The massive vein sample (CV-14PE), which was taken from the Pasir Ela area, is characterized by high metal contents (1.23 ppm Au, 46.9 ppm Ag, 12,100 ppm Cu, 700 ppm Pb, 3,700 ppm Zn). Fluid inclusions in the sample are typically small (3–5 μm), and are dominantly ellipsoidal and rectangular. Necking can be well observed in this sample and both L- and LV-type FIs were found.

Fluid Inclusion Microthermometry

This analysis was conducted to determine the temperatures of melting (T_m), homogenization (T_h) and salinity. The T_m and T_h for the comb-vein FIs are -0.3 to -0.1°C and 245–205°C, respectively. Salinity ranges from 0.18 to 0.53 wt.% NaCl eq. The T_m , T_h and salinity for the lattice bladed-vein FIs are -0.2°C, 230–237°C and 0.36 wt.% NaCl eq., respectively. The T_m , T_h , and salinity for the breccia-vein FIs are -0.6 to -0.3°C, 238–263°C, and 0.53–1.07 wt.% NaCl eq. (higher than the previous two samples), respectively. The colloform-vein FIs also have higher T_h (231–293°C), whilst its T_m and salinity are -1.2 to -0.1°C and 0.18–2.13 wt.% NaCl eq., respectively. The highest FI salinity (1.07–1.60 wt.% NaCl eq.) is found in the massive vein sample, with its T_h and T_m being 274–286°C and -0.9 to -0.6°C, respectively. Microthermometric data and some important petrographic images of fluid inclusions hosted by Cibeber quartz veins are shown in Figure 8.

INTERPRETATION AND DISCUSSION

Alteration/mineralization Paragenetic Sequences

Based on hydrothermal mineral assemblages and field/microscopic crosscutting relationships, the paragenetic sequences of alteration/mineralization can be divided into four major stages (modified from Dana *et al.*, 2018a) namely (I) early-ore, (II) medium-ore, (III) late-ore, and (IV) supergene (Figure 9).

Stage I is characterized by the formation of massive veins with abundant base metal sulfides (*e.g.* galena, sphalerite, and chalcopyrite), together with minor gold and silver sulfides. Gold inclusions in pyrite indicate that gold is formed before pyrite, whilst some samples show that silver sulfides replaced pyrite.

Stage II is characterized by the formation of colloform-crustiform and breccia veins; this is the main Au-Ag mineralization stage. Base metal sulfides are also common but less abundant than in Stage I. Ore textures indicate that Stage II pyrite

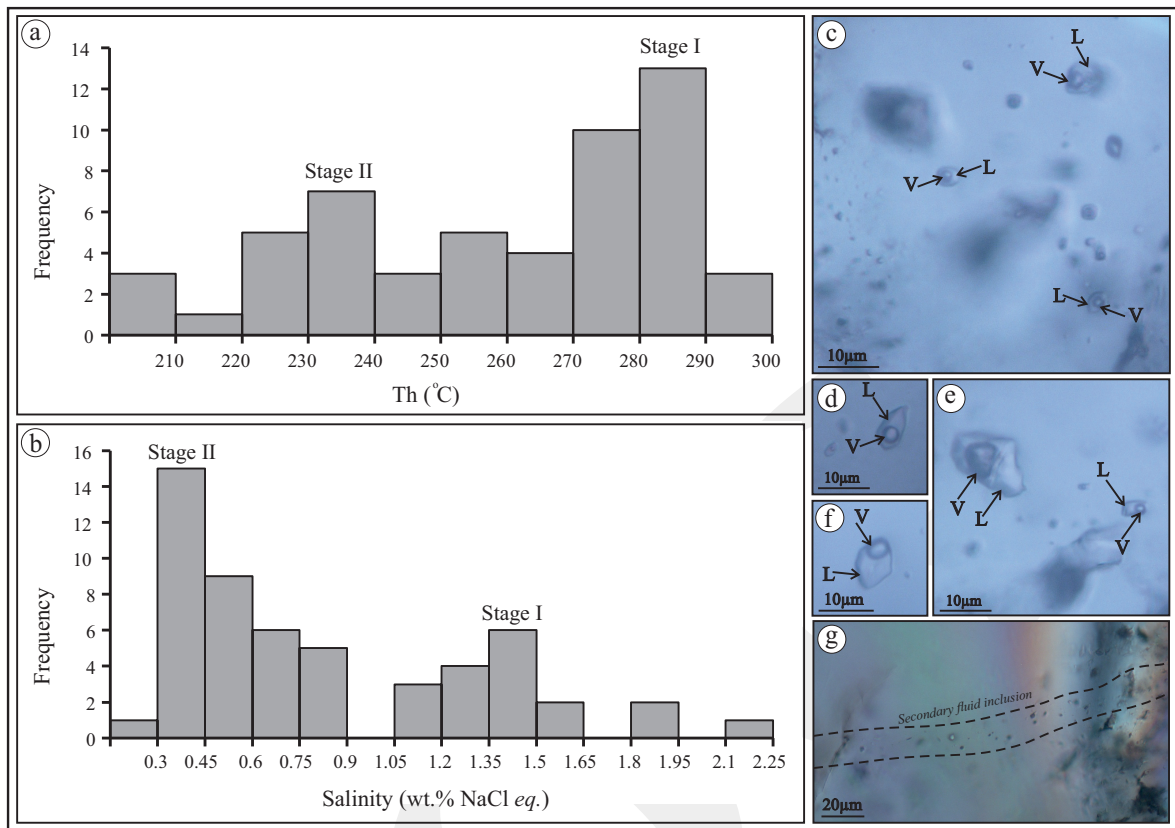


Figure 8. Histograms of (a). Homogenization temperature, showing two peaks at 230 - 240°C and 280 - 290°C, (b). salinity of FIs from quartz showing two peaks at 0.30 - 0.45 wt.% and 1.35-1.50 wt.% NaCl eq., suggesting two main hydrothermal stages (I and II). Stage I associated with massive-/colloform-vein formation was of higher temperature and salinity. Stage II associated with lattice-/comb-textured vein formation was of lower temperature and salinity, probably resulted from mixing with meteoric water. Highest Tm (up to 293°C) and salinity (up to 2.13 wt.% NaCl eq.) are found in a massive vein sample (CV-14PE); (c-g). Petrography of fluid inclusion from Cibeber epithermal quartz veins; (c). Biphase fluid inclusion assemblage from massive vein (CV-14PE); (d, f). Ellipsoid biphase LV fluid inclusions from colloform vein (CV-02PE); (e). Rectangular biphase LV fluid inclusion from comb vein (CV-01CJ); (g). Secondary fluid inclusion trail from breccia vein sample (CV-12LD).

mostly replaces Stage I base metal sulfides. Stage II chalcopyrite and galena are formed before sphalerite, as indicated by replacement texture. The presence of chalcopyrite disease texture indicates that some chalcopyrite coprecipitated with the sphalerite (*e.g.* Schwartz, 1951; Craig and Vaughan, 1994; Inesom, 1989).

Stage III is characterized by the formation of comb-/bladed-/saccharoidal-textured barren veins, which are typically found in the uppermost part of epithermal mineral systems (*e.g.* Wilson and Tunningley, 2013). Mineralization is insignificant, except for some pyrite, rare gold, and silver sulfides.

Stage IV is characterized by the replacement of hypogene minerals by supergene minerals,

such as covellite, malachite, hematite, and goethite.

In terms of alteration zoning, the silicic zone was formed before the argillic and propylitic zones. Hydrothermal quartz was deposited throughout the various alteration stages, whilst cristobalite was formed only in Stage I to II. Clay minerals (mostly illite) were formed in Stage II and propylitic minerals such as chlorite, epidote, and calcite in Stage III.

Sulfidation State and Deposit Type

Epithermal deposits have been divided into low-/intermediate-/high-sulfidation (LS, IS, HS) types (*e.g.* Hedenquist *et al.*, 2000; Einaudi *et al.*, 2003; Sillitoe and Hedenquist, 2003; Simmons *et*

| Ore minerals/ gangue/ alteration | Mineralization Stages | | | | | | |
|--|-----------------------|-----------|-------------------|---------|--------------|-------|-----------|
| | 280°C | | 275°C | | 220°C | | Supergene |
| | Early | | Middle | | Late | | |
| | Qz-base metal | | Qz-precious metal | | Qz-carbonate | | |
| Texture | Masif | Colloform | Breccia | Lattice | Comb | | |
| Ore | | | | | | | |
| Gold | | | | | | | |
| Ag-sulfide | | | | | | | |
| Pyrite | | ————— | | | | | |
| Chalcopyrite | ————— | | | | | | |
| Galena | | | ————— | | | | |
| Sphalerite | ————— | | | | | | |
| Tennantite | | | ————— | | | | |
| Tetrahedrite | | | ————— | | | | |
| Covellite | | | | | | ————— | |
| Malachite | | | | | | ————— | |
| Hematite | | | | | | ————— | |
| Goethite | | | | | | ————— | |
| Gangue/ Alteration | | | | | | | |
| Quartz | ————— | | | | | | |
| Crystobalite | | ————— | | | | | |
| Illite | | ————— | | | | | |
| Epidote | | | | ————— | | | |
| Chlorite | | | | ————— | | | |
| Calcite | | | | | | ————— | |

Figure 9. Paragenetic sequences of alteration and mineralization stages of Cibeber deposits (modified from Dana *et al.*, 2018).

al., 2005; Hedenquist and Arribas, 2017). Binary plots between homogenization temperature and salinity within Wilkinson (2001) deposit type classification indicate that the mineralization in the researched area can be categorized as an epithermal, because of its low temperature and salinity. Our FI homogenization temperature and salinity data indicate that the epithermal mineralization is of high- to low-S type (cf. Bodnar *et al.*, 2014).

Binary plot of Au vs. Ag grade indicates that the samples from Cibeber can be divided into two groups. High Ag:Au samples come mostly from the southern Cibeber (at/around Pasir Ela), whereas the northern Cibeber (at/around Lebak Dadap) is characterized by low Ag:Au samples (Figure 10). IS epithermal deposits commonly have higher Ag:Au ratios than their LS counterparts (Einaudi *et al.*, 2003; Gemmill, 2004).

Thus, the mineralization is proposed to change from IS in southern Cibeber to LS in northern Cibeber. An IS state of mineralization in southern Cibeber (Figure 11) is further supported by the absence of arsenopyrite and abundance of base-metal sulfides (Giggenbach, 1997; Einaudi *et al.*, 2003).

Sphalerite from Cibeber can be divided into low-Fe (<10 mol% FeS) and high-Fe (>10 mol% FeS) type. IS deposits typically have low-Fe sphalerite while LS deposits have high-Fe one (Einaudi *et al.*, 2003). The low-Fe and high-Fe sphalerite from Cibeber have 3.07–3.89 and 11.03–11.82 mol% FeS, respectively, and thus both low- and intermediate-S epithermal systems are present in the studied area. The low-S epithermal system is typically found in northern Cibeber as indicated by lack occurrence of base

Geology, Vein Textures, and Fluid Inclusions of the Cibeber Low-Intermediate Sulfidation Epithermal Au-Ag Orefield, Western Java (C.D.P. Dana *et al.*)

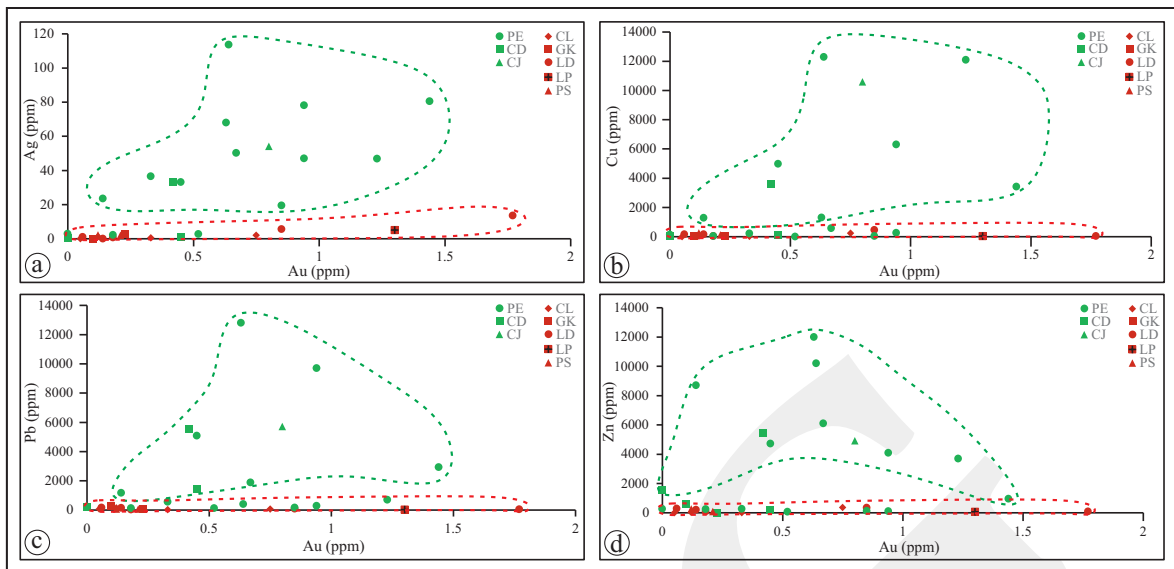


Figure 10. Binary plot of gold grade vs other metal grade: (a) Au/Ag, (b) Au/Cu, (c) Au/Pb, and (d) Au/Zn at Cibeber goldfield showing the data fall clearly into two main groups i.e. low sulfidation epithermal (red symbols), and intermediate sulfidation epithermal (green symbols). The high Ag:Au ratio is typical of intermediate-sulfidation epithermal deposits. Abbreviation: PE: Pasir Ela; CD: Cidikit; CE: Curug Engang; CJ: Citajin; LP: Lamping; LD: Lebak Dadap; PS: Pasir Suung; GK: Gunung Keris; CL: Cilulumpang.

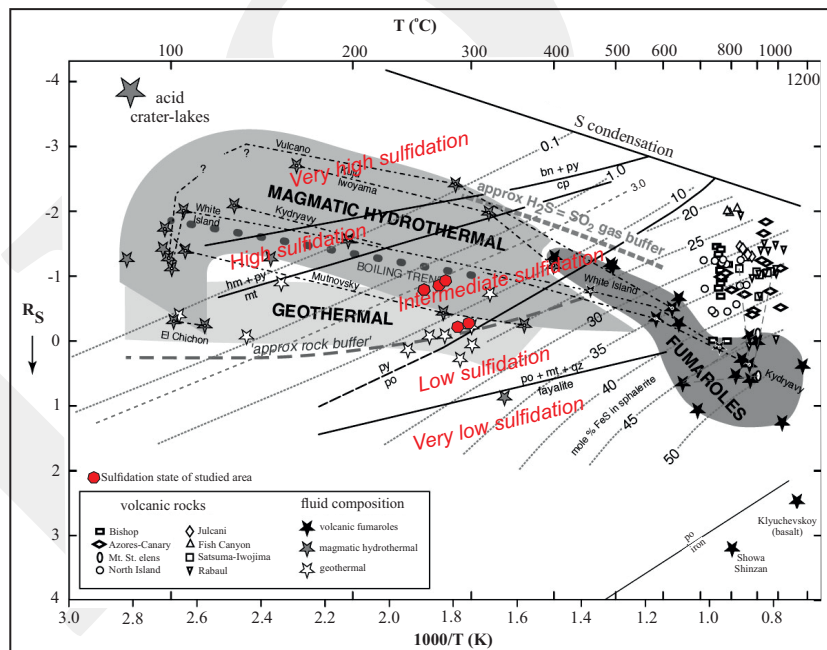


Figure 11. Estimated sulfidation state of the Cibeber epithermal deposits based on formation temperature and Fe content in sphalerite (diagram after Einaudi *et al.*, 2003).

metal-bearing minerals, whereas the intermediate-S epithermal system is in southern Cibeber as indicated by the abundance of base metal-bearing minerals. The Fe content of sphalerite from northern Cibeber is also typically lower than those which come from southern Cibeber.

Fluid Source And Evolution

Hydrothermal fluid changes can be estimated by the fluid inclusion homogenization temperature vs. salinity plot (Figure 12; Shepherd *et al.*, 1985), which indicate two major hydrothermal evolution processes in the studied area: (1) simple cooling

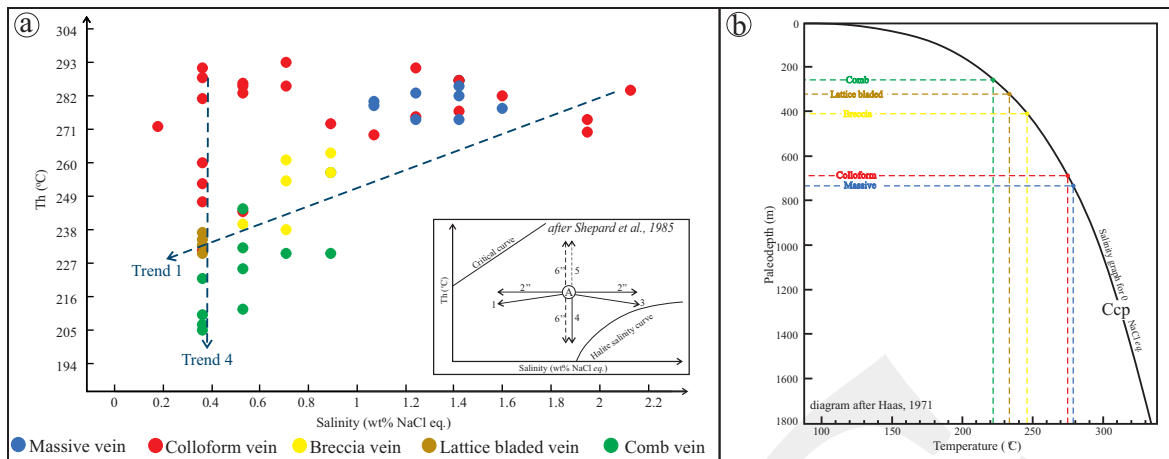


Figure 12. (a) Fluid inclusion Th vs. salinity diagram, showing two distinctive trends (No. 1 and 4; Shepard *et al.* 1985) that represent two distinct fluid evolution processes: Trend 1 and 4 represent mixing with lower-temperature/-salinity fluid and simple cooling, respectively. (Explanation of each trend: (1) mixing with cooler and lower salinity fluid (2) isothermal mixing with fluid which has highly contrast salinity (3) boiling with slower cooling process (4) simple cooling (5) inclusion leaking during heating process (6) necking down. (b) Correlation plot of homogenization temperature and paleo-depth of vein formation (after Haas 1971). It shows that the massive- and colloform veins were formed at deeper level than the breccia-, lattice bladed and comb veins.

caused by the interaction between hydrothermal fluid with the cooler wall rock, and (2) mixing with a cooler and less saline fluid, *e.g.* meteoric water. Fluid inclusions from the massive-/colloform-/breccia veins indicate higher fluid temperatures and salinity than those from the comb-/lattice bladed veins. This suggests that the latter may have formed via fluid mixing. In Figure 12, it is also shown that there may have been two fluid sources. The first source may have been meteoric water (as indicated by its low salinity), which was heated by a deep-seated intrusion. The fluid may have only undergone simple cooling during its evolution. However, an indication of a boiling process can also be identified in colloform and breccia veins (*e.g.* Guoyi *et al.*, 1995). This fluid was likely the ore-forming fluid. The second fluid was likely resulted from mixing of the first fluid with the circulating meteoric water and may have formed the Stage III barren veins.

Genetic Model

Integrating field deposit geology, mineralogy, geochemistry, and hydrothermal fluid features, the following genetic model was proposed for the Cibeber deposits (Figure 13). The Cibeber epithermal deposits are hosted in a Paleogene

volcanic centre. A previous study mentioned that the abundance of mineral deposit in this area is mostly controlled by advanced magma evolution that increases the alkali content of the magmatic-hydrothermal system (Setijadji *et al.*, 2006). The mineralization is interpreted to have occurred during the Mio-Pliocene period based on K-Ar dating from surrounding areas (McInnes *et al.*, 2004; Yuningsih *et al.*, 2014). Syn-ore structures are likely the result of subduction activity in southern Java as indicated by the lineament pattern, while the pre-ore structures are associated with caldera formation in the Bayah Dome Volcanic Complex as suggested by the presence of a regional circular (caldera-like) structure.

Limited input from magmatic fluids suggests a distal heat source, possibly outside the studied area. The pressure vs. mineralization depth plot (Haas, 1971) (Figure 12) indicates that the mineralization depth was around 258 - 700 m below the paleosurface when the pressure was about 28 - 55.1 bar. The positive silver vs. base metal grade correlation indicates that these metals are cogenetic. Positive gold vs. silver grade correlation indicates that the two metals occur possibly as electrum rather than as native metals. Higher gold grades are typically found in colloform and

breccia veins, whilst breccia veins are commonly silver-rich (Figure 14). Higher base metal contents are typically found within massive veins. Other vein textures (*e.g.*, lattice bladed, comb,

and saccharoidal) typically have lower ore grades. These features suggest that the gold-rich veins were formed at a deeper level than the silver-rich ones, whereas the low-grade and ore-barren veins

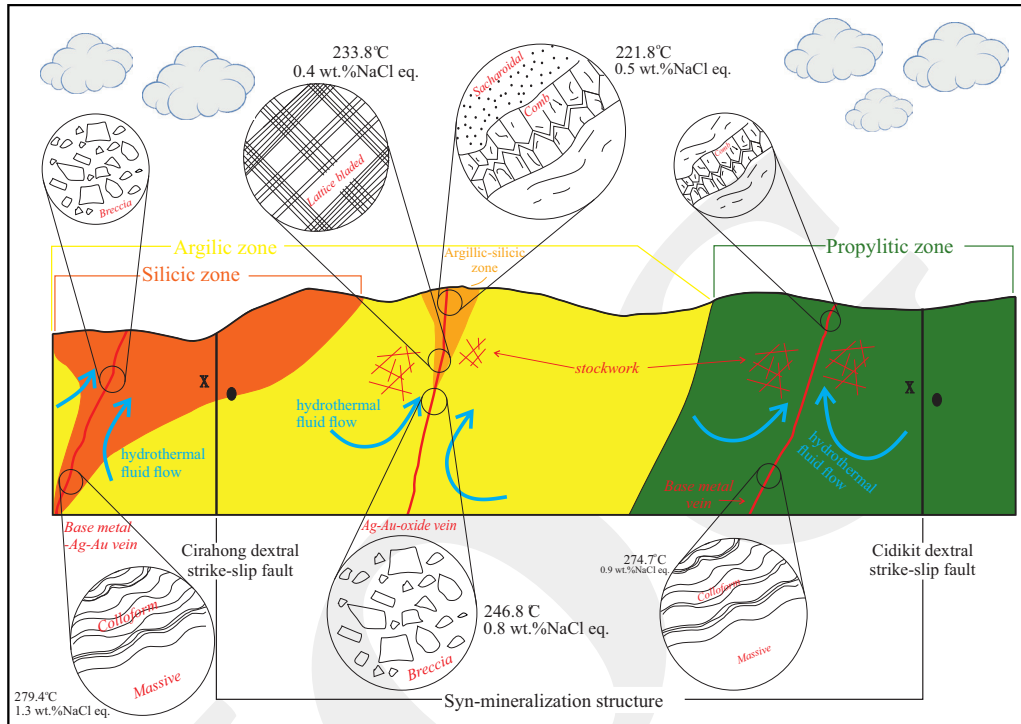


Figure 13. Schematic genetic model of the Cibeber deposits. The model shows that the hydrothermal fluid was mainly sourced from meteoric water, and its circulation was driven by an external heat source, probably a deep-seated pluton outside Cibeber. The different fluid flow regimes at different depths in the various alteration zones have formed the different vein textures.

| Epithermal stage | | Early → Late | | | | | | |
|------------------|----------------------|-----------------|-----------------|-----------------|-------------------------|-------------------------|----------------|----------------|
| Vein texture | | | | | | | | |
| | | Massive | Colloform | Breccia | Lattice bladed | Stockwork | Comb | Saccharoidal |
| Ore minerals | | Py, Ccp, Gn, Sp | Py, Ccp, Gn, Sp | Pyrite, Chalco- | Pirit, hematit, goethit | Pirit, hematit, goethit | Pirit, hematit | Pirit, hematit |
| | | | | | | | | |
| Ore grade | Au | 0.73 ppm | 1.54 ppm | 1.10 ppm | 0.35 ppm | 0.29 ppm | 0.22 ppm | 0.17 ppm |
| | Ag | 35.24 ppm | 36.31 ppm | 36.38 ppm | 1.33 ppm | 5.75 ppm | 0.73 ppm | 0.6 ppm |
| | Base metal | Zn Pb Cu | | | | | | |
| Fluid | Temp. (°C) | 279.38 | 274.72 | 246.88 | 233.75 | n/a | 221.80 | n/a |
| | Salinity (wt.% NaCl) | 1.31 | 0.90 | 0.76 | 0.36 | n/a | 0.52 | n/a |

Figure 14. Evolution of vein texture and mineral assemblages, ore grade and fluid temperature and salinity from the early- to late-stage epithermal mineralization at Cibeber. Relation between vein texture and ore grade is also shown.

were formed at the shallowest level. Since fluid inclusion data can reveal fluid trapping conditions (Bodnar, 2003), Au-Ag mineralization likely occurred at 245–275°C (coeval with colloform-/breccia-veining). Based on published hydrothermal mineral stabilization temperatures (Henley *et al.*, 1984; Reyes and Giggenbach, 1992; White and Hedenquist, 1995; Zhu *et al.*, 2011), Stage III ore mineralization temperatures are estimated to be 225–265°C, while supergene mineralization occurred at 140–200°C.

CONCLUSIONS

The Cibeber epithermal deposits are hosted by the Cikotok Formation in the Bayah Dome complex, structurally controlled by NE-trending faults. Low- and intermediate-sulfidation mineralization styles are found in the northern- and southern Cibeber, respectively. Hypogene hydrothermal processes can be divided into early Au-Ag-dominated mineralization, middle base metal-dominated mineralization, and late ore-barren hydrothermal veining stages. Fluid inclusion evidence suggests that the ore-forming fluids have had relatively low temperature and salinity sourced mainly from meteoric water, with their circulation being driven by a concealed heat source, possibly a deep-seated pluton outside Cibeber. The vein texture-ore grade-hydrothermal fluid correlation established in the current study will be a useful guide for further exploration in this area and surroundings. However, detailed mineral chemistry and whole rock geochemistry of the host rock need to be carried out to determine the geochemical signature of the deposits.

ACKNOWLEDGEMENTS

This study was financially supported by the Undergraduate Thesis Programme Research Grant 2018 of Universitas Gadjah Mada to the second author, and the Kageogama Hardrockers of Economic Geology Professional Association

of UGM Geological Engineering Alumnae and Beasiswa 2003 and Sahabat of UGM Geological Engineering Alumnae Batch 2003 Foundation. The authors thank Rudy and Agam Mujahid for helping with the FA-AAS analyses, and the staffs from PT Multi Utama Kreasindo Mining for the field assistance. Special thank goes to Laurie Whitehouse for the valuable discussion and language editing.

REFERENCES

- Angeles, A.C., Prihatmoko, S., and Walker, J.S., 2002. Geology and alteration-mineralization characteristics of the Cibaliung epithermal gold deposit, Banten, Indonesia. *Resource Geology*, 52 (4), p.329-339. DOI:10.1111/j.1751-3928.2002.tb00143.x
- Barker, A., 2014. *A key for identification of rock-forming minerals in thin section*. CRC Press, London, 170pp.
- Bemmelen, R.W., 1949. *The geology of Indonesia. 1A, General geology of Indonesia and adjacent archipelagoes*. 766 pp. Government Printing Office, Martinus Nijhoff, The Hague.
- Bodnar R.J., Lecumberri-Sanchez P., Moncada D., and Steele-MacInnis M., 2014. Fluid Inclusions in Hydrothermal Ore Deposits. *In: Holland, H.D. and Turekian, K.K. (eds.), Treatise on Geochemistry*, Second Edition 13, 650pp. Elsevier, Oxford, p.119-142. DOI:10.1016/b978-0-08-095975-7.01105-0
- Bodnar, R.J., 2003. Introduction to fluid inclusion: Analysis and interpretation. *Mineral Association Canada, Short Course*, 32, p.1-8.
- Chen, P., 1977. Table of key lines in X-ray powder diffraction patterns of minerals in clays and associated rocks. *Department of Natural Resources Geological Survey Occasional Paper*, 21, p.1-67.
- Corbett, G., 2013. World Gold Pacific Rim Epithermal Au-Ag. *Proceedings of the World Gold Conference, Brisbane*. . DOI:10.5382/sp.06
- Corbett, G.J. and Leach, T.M., 1996. Southwest Pacific Rim gold-copper systems: structure,

- alteration, and mineralization. 145 pp. *A workshop presented for Society of Exploration Geochemists at Townsville.*
- Craig, J.R. and Vaughan, D.J., 1994. *Ore microscopy and ore petrography, Second Edition.* John Wiley and Sons, USA, 434pp.
- Dana, C.D.P., Idrus, A., Yuniardi, F., Meak, I.A., and Langkoke, R., 2018a. Mineralogi dan Tekstur Endapan Emas Epitermal Sulfidasi Rendah Menengah Daerah Cibeber, Kompleks Kubah Bayah, Provinsi Banten. *Proceedings, Seminar Nasional Kebumihan, Yogyakarta*, p.695-706.
- Dana, C.D.P., Idrus, A., Yuniardi, F., Meak, I.A., and Masti, S.D., 2018b. Geology and Hydrothermal Alteration of Cibeber Prospect, Lebak, Banten: A preliminary study of Au-Ag-base metal sulfide deposit. *Proceedings of EAGE-HAGI 1st Asia Pacific Meeting on Near Surface Geoscience and Engineering 2018. Yogyakarta*, p.1-5. DOI:10.3997/2214-4609.201800353
- Einaudi, M.T., Hedenquist, J.W., and Inan, E.E., 2003. Sulfidation state of fluids in active and extinct hydrothermal systems: Transitions from porphyry to epithermal environments. *Special Publications, 10, Society of Economic Geologists*, p.285-313. DOI:10.5382/sp.10.15
- Garwin, S., 2013. Tectonic and structural controls to porphyry and epithermal mineralization in cenozoic magmatic arcs of SE Asia and the W Pacific: AIG Annual Meeting. 36 pp. *Keynote Lecture at CET Seminar Series, UWA, Perth.*
- Gemmell, J.B., 2004. *Low- and intermediate-sulfidation epithermal deposits: ARC-AMIRAP. Australia*, p.57-63.
- Giggenbach, W.F., 1997. The origin and evolution of fluids in magmatic-hydrothermal systems. *In: Barnes, H.L. (eds.), Geochemistry of Hydrothermal Ore Deposits, Third Edition*, 958pp. John Wiley and Sons, USA, p.737-796.
- Goldstein, R.H., 2003. Petrographic analysis of fluid inclusions. *In: Samson, I., Anderson, A., and Marshall, D. (eds.), Fluid Inclusions: Analysis and Interpretation Short Course.* Mineral Association Canada, 32, p.9-53. DOI:10.1007/s00126-004-0411-6
- Guoyi, D., Morrison, G., and Jaireth, S., 1995. Quartz texture in epithermal veins. Queensland-Classification Origin and Implication. *Economic Geology*, 90, p.1841-1856. DOI:10.2113/gsecongeo.90.6.1841
- Haas, J.L., 1971. Effect of salinity on the maximum thermal gradient of a hydrothermal system at hydrostatic pressure. *Economic Geology*, 66, p.940-946. DOI:10.2113/gsecongeo.66.6.940
- Harijoko, A., Ohbuchi, Y., Motomura, Y., Imai, A., and Watanabe, K., 2007. Characteristics of the Cibaliung gold deposit: miocene low-sulfidation-type epithermal gold deposit in Western Java, Indonesia. *Resource Geology*, 57 (2), p.14-123. DOI:10.1111/j.1751-3928.2007.00011.x
- Hedenquist, J.W., 2000. Exploration for epithermal gold deposits. *Review in Economic Geology*, 13, p.245-277.
- Hedenquist, J.W. and Arribas, A., 2017. Epithermal ore deposits: first-order features relevant to exploration and assessment. *Proceedings of 14th SGA Biennial Meeting, 1, Quebec, Canada*, p.47-50.
- Henley, R.W., Truesdell, A.H., Barton, P.B., and Whitney, J.A., 1984. *Fluid-mineral equilibria in hydrothermal systems.* Society of Economic Geologists, 267pp. DOI:10.5382/rev.01
- Hutabarat, J., 2016. Geokimia batuan vulkanik formasi Cikotok di segmen utara kubah Bayah, Banten. *Bulletin of Scientific Contribution, Faculty of Geological Engineering, Padjajaran University, Bandung*, 14 (2), p.195-204.
- Ineson, P.R., 1989. *Introduction to practical ore microscopy*, Longman Group Ltd., New York, 192pp.
- Leeuwen, T.V., 1994. 25 years of mineral exploration and discovery in Indonesia. *In: Mineral deposits of Indonesia: Discoveries of the past 25 years. Journal of Geochemical Exploration*, 50, 1390pp. DOI:10.1016/0375-6742(94)90021-3

- Marcoux, E. and Milesi, J.P., 1994. Epithermal gold deposits in West Java, Indonesia: geology, age and crustal source. *Journal of Geochemical Exploration*, 50, p.393-408. DOI:10.1016/0375-6742(94)90033-7
- Marshall, D., Anglin, C.D., and Mumin, H., 2004. *Ore mineral atlas*. Geological Association of Canada, 112pp.
- McInnes, B.I.A., Evans, N.J., Sukarna, D., Permanadewi, S., 2004 Thermal histories of Indonesian porphyry copper-gold deposits determined by U-Th-He, U-Pb, Re-Os, K-Ar and Ar-Ar methods. *Extended Abstracts, SEG*, p.343-346.
- Pirajno, F., 2010. *Hydrothermal processes and mineral systems*. Springer Science and Business Media, Perth, 1273pp.
- Pohl, W.L., 2011 *Economic geology principles and practice: Metals, minerals, coal, and hydrocarbons - introduction to formation and sustainable exploitation of mineral deposits*. John Wiley and Sons, West Sussex, 699pp. DOI:10.1002/9781444394870
- Potter R.W., 1977. Pressure corrections for fluid-inclusion homogenization temperatures based on the volumetric properties of the system NaCl-H₂O. *Journal of Research USGS*, 5, p.603-607.
- Prihatmoko, S. and Idrus, A., 2020. Low-sulfidation epithermal gold deposits in Java, Indonesia: Characteristics and linkage to the volcano-tectonic setting. *Ore Geology Reviews*, 121, 103490. DOI:10.1016/j.oregeorev.2020.103490
- Pulunguno, A. and Martodjojo, S., 1994. Perubahan tektonik paleogen-neogen merupakan peristiwa tektonik terpenting di Jawa. *Proceedings of Geologi dan Geodinamik Pulau Jawa, Faculty of Engineering, UGM*, p.37-55.
- Reyes, A.G. and Giggenbach, W.F., 1992. Petrology and fluid chemistry of magmatic-hydrothermal systems in the Philippines, In Water Rock Interaction. *Proceedings of the 7th International Symposium on Water-Rock Interaction*. Park City, USA, Balkema, Rotterdam, p.1341-1344.
- Rosana, M.F., 2009. Karakteristik mineralisasi logam di kawasan Jawa bagian barat. *Monthly Seminar at Faculty of Geological Engineering, Padjajaran University*, 7pp.
- Schwartz, G.M., 1951. Classification and definitions of textures and mineral structures in ores, *Economic Geology*, 46. p.578-591. DOI:10.2113/gsecongeo.46.6.578
- Setidjaji, L.D., Kajino, S., Imai, A., and Watanabe, K., 2006. Cenozoic Island Arc Magmatism in Java Island (Sunda Arc, Indonesia): clues on relationship between geodynamics of volcanic centre and ore mineralization. *Resource Geology*, 56 (3), p.267-292. DOI:10.1111/j.1751-3928.2006.tb00284.x
- Shepherd, T.J., Rankin, A.H., and Alderton, D.H.M., 1985. *A practical guide to fluid inclusion studies*. Blackie, The United Kingdom, 222pp.
- Sillitoe, R.H. and Hedenquist, J.W., 2003. Linkages between volcanotectonic settings, ore-fluid compositions, and epithermal precious-metal deposits. In: Simmons, S.F. and Graham, I. (eds.), *Volcanic, geothermal, and ore-forming fluids: rulers and witnesses of processes within the earth Special Publication*, 10, Society of Economic Geologists, p.315-343. DOI:10.5382/sp.10.16
- Simmons, S.F., White, N.C., and John, D.A., 2005. Geological characteristic of epithermal precious and base metals deposits. *Economic Geology 100th Anniversary Volume*, p.485-522. DOI:10.5382/av100.16
- Sujatmiko and Santosa, S., 1992. *Peta Geologi Lembar Leuwidamar, Jawa skala 1: 100.000*. Pusat Penelitian dan Pengembangan Geologi, Indonesia.
- Sunarya, Y., 1997. Potensi dan prospek emas di Jawa Barat. *Special Publication of Directorate of Indonesian Mineral Resources*, 19pp.
- Terry, R.D. and Chillingar, G.V., 1995. Comparison chart for visual percentage estimation. www.farallones.org.
- Warmada, I.W., 2003. *Ore mineralogy and geochemistry of the Pongkor epithermal gold-silver deposit, Indonesia*. Ph.D. thesis, Insti-

- tute of Mineralogy and Mineral Resources, Technical University of Clausthal, Zellerfeld, Germany, 107pp.
- White, N.C. and Hedenquist, J.W., 1995. Epithermal gold deposits: styles, characteristics and exploration. *SEG Newsletter*, 23, p.19-13.
- Whitford, D.J., 1975. *Geochemistry and petrology of volcanic rocks from the Sunda Arc, Indonesia*. Ph.D. thesis, Australian National University, Canberra, Australia, 449pp.
- Widi, B.N., 2007. Model mineralisasi di Daerah Kubah Bayah: suatu pendekatan strategi dalam eksplorasi mineral. Pemaparan Hasil Kegiatan Lapangan dan Non Lapangan. *Proceedings of Pusat Sumber Daya Geologi*, Bandung, 10pp.
- Wilkinson, J.J., 2001. Fluid inclusions in hydrothermal ore deposits. *Lithos*, 55, p.229-272. DOI:10.1016/S0024-4937(00)00047-5
- Wilson, C. and Tunningley, A., 2013. *Understanding low sulfidation epithermal deposits*. Association of Mining Analysts, London, 32pp.
- Yuningsih, E.T., Matseuda, H., and Rosana, M.F., 2014. Epithermal gold-silver deposits in Western Java, Indonesia. Gold-Silver Selenide-Telluride Mineralization. *Indonesian Journal on Geoscience*, 1 (2), p71-81. DOI:10.17014/ijog.v1i2.180
- Zhu, Y.F., An, F., and Tan, J., 2011. Geochemistry of hydrothermal gold deposits. *Geoscience Frontiers*, 2 (3), p.367-374. DOI:10.1016/j.gsf.2011.05.006